Current transport and the fluctuation of critical current in high-temperature superconductor interface-engineered Josephson junctions

Jiro Yoshida, Hiroshi Katsuno, Kohei Nakayama, and Toshihiko Nagano
Advanced Materials and Devices Laboratory, Corporate Research and Development Center, Toshiba Corporation, 1 Komukai Toshiba-cho, Saiwai-ku, Kawasaki 212-8582, Japan
(Received 7 November 2003; revised manuscript received 1 June 2004; published 18 August 2004)

The mechanisms of current transport in interface-engineered junctions (IEJs) with ramp-edge geometry were investigated to clarify the possible origin of the statistical fluctuation of the Josephson critical current. More than 1000 junctions with a ramp edge aligned either along the [100] or [110] axis of the high-temperature superconductor electrode were fabricated under various process conditions. These junctions exhibited a critical current density ranging from 10^2 to 10^6 A/cm^2 at 4.2 K while maintaining a magnetic field modulation of the critical current exceeding 80% without any indication of the peculiar effect of *d*-wave pairing symmetry. The junctions with a critical current density exceeding 10^4 A/cm^2 exhibited an appreciable amount of excess current that grew rapidly within an approximate voltage range of less than 5 mV. The critical current versus temperature characteristics of these junctions were found to be explained reasonably well by a superconductor-normal-superconductor (SNS) junction model in the diffusive regime. This model is also consistent with our observation of a weak subharmonic gap structure due to multiple Andreev reflections. In addition, we found that the Josephson critical current (I_c) exhibited a good correlation with the differential resistance near 0 V, while the normal resistance defined at a current level of two to three times I_c varied appreciably even for junctions with a similar I_c. This indicates that another conduction channel with little contribution to the Josephson current coexists within the junctions. The dI/dV measurement for high resistance junctions revealed that resonant tunneling of quasiparticles through localized states in an insulating barrier constitutes this second conduction channel. All these results suggest that IEJs should be regarded as an array of microscopic SNS contacts embedded in an insulating barrier with random orientation. The fluctuation in the number of SNS contacts in a junction restricts the attainable minimum spread of the I_c value.

DOI: 10.1103/PhysRevB.70.054511 PACS number(s): 74.50.+r, 74.72.−h, 74.45.+c, 85.25.Cp

I. INTRODUCTION

The uniformity and reproducibility of junction characteristics still constitute the major challenge facing high-temperature superconductor Josephson junction technology for digital circuit applications. The interface-engineered junctions (IEJs) proposed by Moeckly and Char seem to be most promising in this regard.[1] The basic concept concerning fabrication of an IEJ is to create a thin barrier layer on the ramp edges by damaging the $YBa_2Cu_3O_7$ (YBCO) base electrode surface using ion bombardment and then recrystallizing the surface into a barrier during the subsequent counter-electrode deposition process. Moeckly and Char have utilized low-temperature annealing of YBCO ramp edges at 400–600 °C in vacuum for 30 min followed by plasma treatment of the surface for several minutes in a 10–100 mTorr Ar/O_2 mixture gas to create the barrier layer. Junctions fabricated by this process have exhibited clear Josephson characteristics appropriate for single-flux-quantum logic circuit applications. The standard deviation σ of the Josephson critical current (I_c) has been reported to be as low as 7.8% over ten junctions in a chip, which is far superior to the values reported for any of the other junctions with an artificial barrier.[2]

The high uniformity of IEJs has been verified further by the subsequent work of Satoh and his co-workers,[3] though their fabrication process differed considerably from that of Moeckly and Char. They found that even a conventional ion-milling process to form the ramp-edge structure followed by counter-electrode deposition in appropriate conditions was sufficient to create an interface barrier. The standard deviation of I_c in this type of IEJ was 8% for a 100-junction array in a chip at 4.2 K. Since then, several groups have pursued this approach aiming at a further reduction in the I_c spread, and have reported σ values as low as 5.7% for 100 junctions and 7.3% for even a 1000-junction array.[4]

In spite of such progress in fabrication technology, however, neither the structure of the interface barrier nor the current transport in IEJs is well understood. It has been recognized that the ion-milling process produces a Y-rich amorphous layer with a thickness of a few nm on the ramp edges.[5] Early transmission electron microscopy and microanalysis studies on IEJs with a relatively low Josephson critical current density (J_c) have indicated that the amorphous layer turns into a 2- to 3-nm-thick continuous well-crystallized barrier with cubic or pseudo-cubic symmetry covering the ramp-edge surface without any detectable pinholes.[5,6] However, more recent studies have clarified that such a well-defined barrier disappears in high-J_c junctions with J_c exceeding 10^5 A/cm^2.[7–9] These results indicate that the microstructure of the junction interface is process dependent, and thus various current transport mechanisms may coexist within the junction. It is highly probable that the relative importance of the individual mechanisms differs among junctions depending on the fabrication process. In fact, some authors have already pointed out that resonant tunneling of quasiparticles plays an important role in low-J_c junctions, while a metallic channel dominates the Josephson current in high-J_c junctions.[10,11]

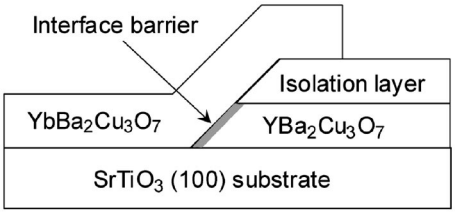

FIG. 1. Schematic representation of an interface-engineered Josephson junction with ramp-edge geometry.

Another important issue that has to be addressed is the effect of the *d*-wave pairing symmetry in high-temperature superconductors on the Josephson characteristics. A microscopic theory for the Josephson current in anisotropic superconductor junctions in the clean limit with arbitrary interface transparency has been developed fully, and various peculiar features originating from the angular dependent order parameters have been predicted.[12–15] An important consequence of the theory is the anomalous behavior of the Josephson current in terms of its magnitude and its temperature dependence in junctions with a specular interface that has a nonzero angle α relative to the *a* axis of high-temperature superconductors. Experimental observation of this peculiar phenomenon, however, is still controversial.[16–19] Rather, the behavior of some grain boundary junctions.[16–20] seems to be consistent with the phenomenological theory of Sigrist and Rice.[21] This certainly requires a rational explanation.

In this paper, we report the results of a detailed study of current transport in IEJs based on more than 1000 junctions that we have fabricated and tested so far, and discuss a possible junction model that can account for the overall features of the observed junction characteristics. Attention is also paid to the possible origin of the I_c spread.

II. JUNCTION FABRICATION

IEJs with $YbBa_2Cu_3O_{7-x}$ (YbBCO) as the counter electrode were fabricated on ramp edges formed in 200-nm-thick YBCO base-electrode layers. The junction structure is shown schematically in Fig. 1. An epitaxial $SrTiO_3$, CeO_2, or $SrSnO_3$ film was used for interlayer isolation. We have not observed any significant differences in junction characteristics among junctions with different isolation layers. All the films used in the present work were grown on $SrTiO_3$ (100) substrates using an off-axis sputtering system. The advantage of YbBCO as the counter electrode compared with conventional YBCO is that it can grow with complete *c*-axis orientation in a far wider temperature range than is possible with the other 123 compounds.[22] This enables us to investigate the dependence of the junction characteristics on the substrate temperature for counter-electrode deposition in a wider range without sacrificing the quality of the counter-electrode layer.

Details of our junction fabrication process have been described elsewhere.[22,23] Briefly, ramp-edge structures were produced using a photoresist mask that was reflowed after patterning and Ar-ion milling with substrate rotation during etching. The resultant ramp edges had a taper of 20° independent of the edge orientation in a wafer. After etching, the samples were heated to the temperature for the counter-electrode deposition and maintained at that temperature for 10 min. An activated oxygen flux from an electron cyclotron resonance (ECR) plasma source was supplied during the annealing process. Then, a 300-nm-thick YbBCO layer was deposited and the counter-electrode pattern was formed after covering the wafer surface with a 1-μm-thick Au film. In our standard process, the ramp edge was aligned parallel to the [100] axis of the $SrTiO_3$ substrate (i.e., parallel to the *a* or *b* axis of YBCO), and the junction width was fixed at 4 μm. In addition to these "standard" junctions, we have also fabricated some junctions with [110]-oriented ramp edges for comparison. We denote these junctions as [110] junctions in the present paper.

Empirically, we know that the junction characteristics are sensitive to the substrate temperature for counter-electrode deposition and the power supplied to the ECR plasma source during the annealing process. Other factors that have significant influence on the junction characteristics are the acceleration voltage and the incident angle of the Ar-ion beam utilized for the fabrication of the ramp-edge structure. By varying these process parameters, we have obtained IEJs with a Josephson critical current density ranging from 10^2 to 10^6 A/cm^2. Throughout the present paper, we define the Josephson critical current density J_c as $J_c = I_c/wt$, where w is the junction width and t is the thickness of the base-electrode layer. We have processed more than 80 wafers under various process conditions. Every wafer contains nine chips, and each chip has either 16 individual junctions or a 100-junction array on it. From among the large number of fabricated junctions, only those exhibiting excellent Josephson characteristics with a magnetic field modulation of I_c exceeding 80% at 4.2 K were selected to obtain the reliable data discussed in this paper.

III. EXPERIMENTAL RESULTS AND DISCUSSION

A. Josephson properties of standard junctions

Figure 2 depicts several examples of the current-voltage (*I-V*) characteristics observed at 4.2 K for our standard (i.e., [100]-oriented) IEJs with a critical current density ranging from 4.5×10^5 A/cm^2 [Fig. 2(a)] to 5.8×10^3 A/cm^2 [Fig. 2(d)]. The pale lines in Figs. 2(a)–2(c) represent the *I-V* curves in a high magnetic field applied parallel to the junction interface, and the dotted lines show the hypothetical simple ohmic behavior corresponding to the junction normal resistance R_n defined at a current level of two to three times I_c. It is apparent that the junctions shown in Figs. 2(a)–2(c) exhibit an appreciable amount of excess current I_{ex} at high voltages that grows rapidly within an approximate voltage range of less than 5 mV. The differential resistance R_0 near 0 V, which is defined in Fig. 2(a), is a parameter that characterizes the highly nonlinear *I-V* curves in a magnetic field. The presence of the excess current becomes less noticeable as I_c decreases, and junctions with a Josephson current density of less than 10^4 A/cm^2 exhibit what seem to be deficit-current characteristics. A typical example of this is shown in Fig. 2(d), in which the dash-dot line represents the extrapo-

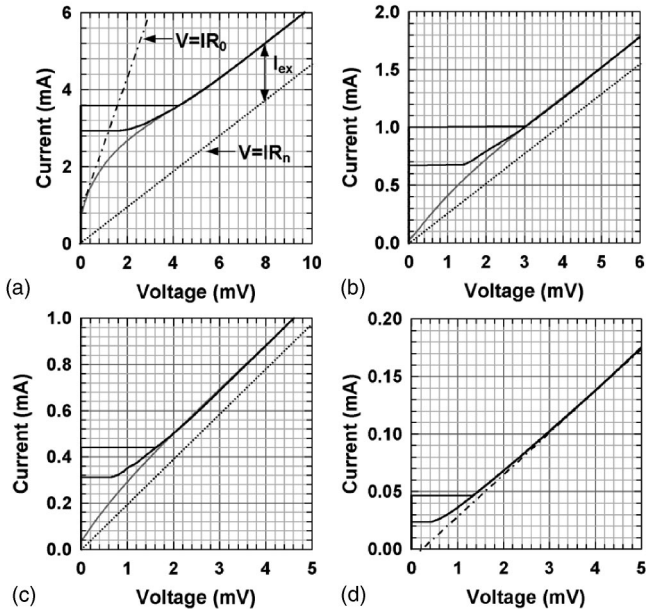

FIG. 2. Current-voltage characteristics observed at 4.2 K for IEJs with a J_c of (a) 4.5×10^5 A/cm^2, (b) 1.3×10^5 A/cm^2, (c) 5.5×10^4 A/cm^2, and (d) 5.8×10^3 A/cm^2, with and without an applied magnetic field that minimizes the zero-voltage current. The dotted lines in (a)–(c) represent hypothetical simple ohmic behavior corresponding to the junction normal resistance R_n. The dash-dot line in (a) defines the differential resistance R_0 near 0 V, while that in (d) is an extrapolation of the quasilinear *I-V* characteristics exhibited at high voltages.

lation of the quasilinear *I-V* characteristics exhibited at high voltages.

Figure 3 shows the magnetic field dependence observed at 4.2 K for the junction whose *I-V* characteristics are shown in Fig. 2(b). The pale line in the figure represents the theoretical Fraunhofer pattern for a junction with uniform current distribution within the junction area. Although the agreement between the theoretical prediction and the experimental result is satisfactory, some discrepancies can be seen in the heights of the higher order maximums in the diffraction pattern. These discrepancies, together with the presence of finite residual currents at the minima, are probably due to inhomogeneities distributed randomly all over the junction interface. The junctions with I_c of less than 1 mA exhibited a more or less similar response to the magnetic field, though the details of the individual diffraction patterns differed from junction to junction, especially in high magnetic fields.

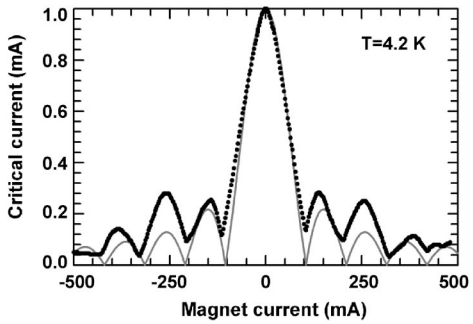

FIG. 3. Magnetic-field modulation of I_c observed at 4.2 K for a junction with a J_c of 1.3×10^5 A/cm^2. The pale line shows the theoretical Fraunhofer pattern for a junction with uniform current distribution.

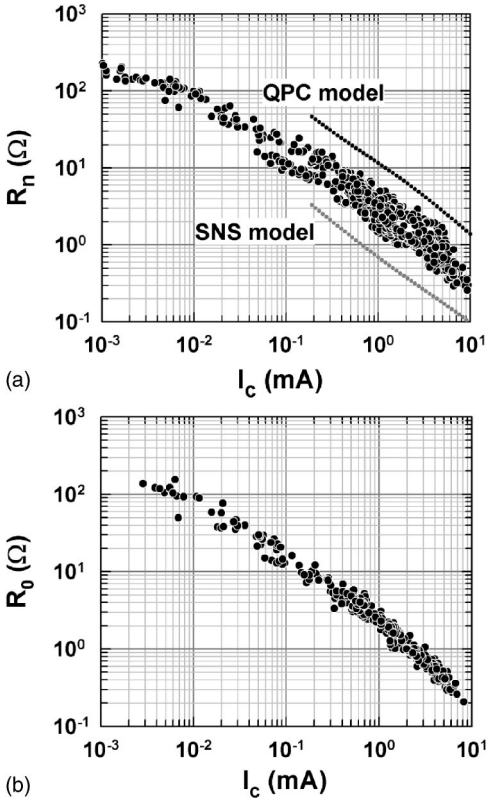

FIG. 4. (a) Correlation between I_c and the junction normal resistance R_n defined at a current level of two to three times I_c. The dark dotted line shows the theoretical prediction based on the quantum point contact (QPC) model, while the pale dotted line corresponds to the SNS model. (b) Similar plot of the differential resistance R_0 near 0 V vs I_c.

The junctions with I_c far exceeding 1 mA behaved differently. These junctions exhibited a magnetic field response typical of a Josephson junction in the large junction regime.[24] The critical currents decreased linearly within a certain magnetic field range, and the residual supercurrent (I_{res}) in a high magnetic field was almost independent of the field strength. I_{res} in a magnetic field of 7300 A/m, which was the maximum field that we could apply in our measurement apparatus, increased gradually with the increase in the I_c in a zero magnetic field, and I_{res}/I_c amounted to more than 15% for junctions with I_c of around 8 mA (i.e., $J_c = 10^6$ A/cm^2). The crossover from small junction behavior to large junction behavior at an I_c of around 1 mA seems to be consistent with the London penetration depth of around 0.2 μm observed for our YBCO and YbBCO films at low temperatures.[23]

Figure 4(a) displays the correlation between the junction normal resistance R_n and I_c at 4.2 K for our standard IEJs with various values of I_c. As mentioned above, we defined R_n as the differential resistance within a current level of two to three times I_c. An interesting feature that can be seen is the

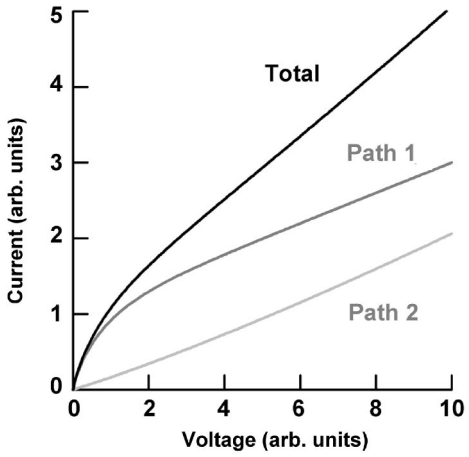

FIG. 5. Current transport paths postulated to coexist in a junction. The total current is given by the sum of the contributions from path 1 and path 2.

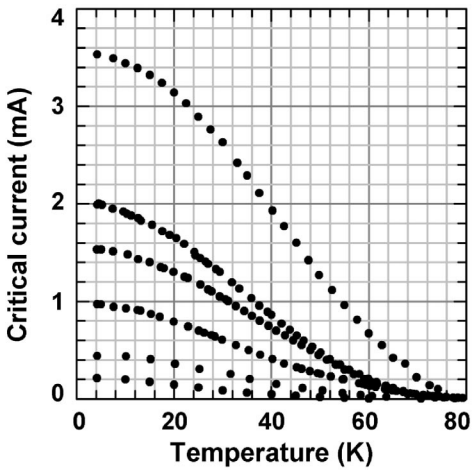

FIG. 6. Temperature dependence of I_c observed for several junctions with J_c larger than 10^4 A/cm^2 at 4.2 K.

large variation in R_n for junctions with similar I_c, especially in the high I_c region. In the case of junctions with an I_c of 1 mA, we notice that the R_n ranges from 1.3 to 5 Ω. Such variations in R_n are certainly beyond any experimental error and suggest that the critical factors influencing I_c and R_n are not identical. In contrast, if we plot the differential resistance R_0 at $V \sim 0$ against I_c, we obtain a far better correlation between them as shown in Fig. 4(b). This implies that I_c and R_0, and thus I_c and I_{exc}, have the same origins.

The experimental results seen in Figs. 4(a) and 4(b) can be reasonably understood by assuming that two kinds of current transport paths coexist in the junctions, as schematically depicted in Fig. 5. One of them (path 1) gives a convex curvature in the *I-V* characteristics and is thus responsible for the excess current. We think that this current path is directly related to the Josephson current. Another path is a channel through a barrier of low transparency, which gives a weak concave curvature in the *I-V* characteristics. We think that this current path plays no significant role in determining the Josephson current, at least in junctions with J_c exceeding 10^4 A/cm^2, except that it works as a shunt resistor embedded within a junction. These current paths will be discussed further in later sections.

Figure 6 shows the temperature dependences of I_c observed for several junctions with J_c larger than 10^4 A/cm^2 at 4.2 K. In spite of the large variation in the absolute I_c values, two general features are evident in the figure. First, all the curves exhibit a weak saturation tendency at low temperatures, which is far weaker than that expected from a simple tunneling theory (Ambegaokar–Baratoff theory) and is close to that expected for the clean weak links described by the Kulik–Omelyanchuk theory.[25] This suggests that the Josephson current in these IEJs flows through a transport channel with a relatively high electron transmission probability. The presence of such a highly transparent channel is consistent with the observation of a large excess current in these junctions.

The second feature evident in Fig. 6 is the "long tails" at high temperatures. We have confirmed that these long tails can be fitted closely either by $(1-T/T_c)^2$ or $(1-T/T_c)^{3/2}$, depending on the I_c value at 4.2 K.[26] Junctions with an I_c of less than 2 mA at 4.2 K generally exhibited $(1-T/T_c)^2$ behavior, while $(1-T/T_c)^{3/2}$ described junctions with a larger I_c better. These peculiar temperature dependences in the vicinity of the critical temperature (T_c) can be understood within the framework of the proximity effect theory. It is known that in superconductor-normal-superconductor (SNS) junctions with a small boundary resistance at the SN interfaces, depairing in the S electrode by the proximity effect results in $(1-T/T_c)^2$ dependence near T_c, and if the N-layer thickness is small enough, depairing in the S electrodes by the supercurrent modifies the temperature dependence to $(1-T/T_c)^{3/2}$.[27] Furthermore, Golubov and Kupriyanov have pointed out that Josephson junctions with thin normal conducting layers on both sides of a tunnel barrier exhibit similar $(1-T/T_c)^2$ dependence near T_c due to the proximity effect, and this dependence changes to $(1-T/T_c)^{3/2}$ when the normal conducting layer on one side of the tunneling barrier disappears.[28] The same authors have also confirmed that these conclusions are valid even if the tunneling barrier is replaced by a microconstriction with arbitrary transparency.[29] Although we cannot infer the types of junctions to which our IEJs belong solely from the temperature dependence of I_c near T_c, it is probable that the local critical temperature T_c^* in the close vicinity of the junction interface becomes low compared with that in the bulk electrodes due to the strain or oxygen deficiency at the interface.

The presence of an appreciable amount of excess current together with the peculiar temperature dependence of I_c mentioned above indicates that a simple superconductor-insulator-superconductor (SIS) or superconductor-normal-insulator-normal-superconductor (SNINS) junction model with an insulator barrier of low transparency is inadequate to describe the junction characteristics, at least for junctions with J_c exceeding 10^4 A/cm^2. Rather, a SNS picture either in the clean limit or in the dirty limit seems to provide a good starting point for further analysis. From this viewpoint, we next look at the junction normal resistance values. Experimentally, the junction resistance R_n was almost independent of temperature or slightly decreasing at low temperatures for

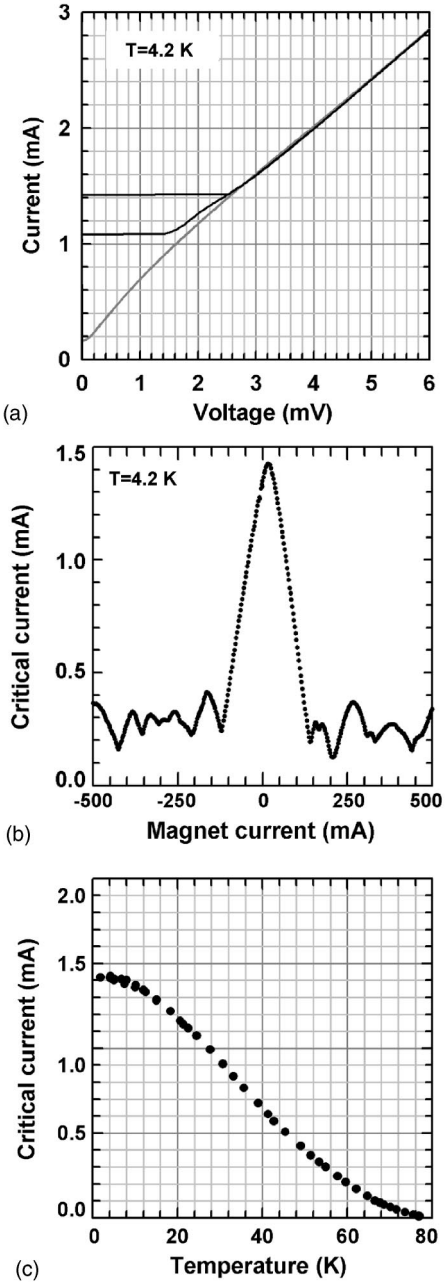

FIG. 7. (a) *I-V* characteristics at 4.2 K with (pale line) and without (dark line) an applied magnetic field. (b) Magnetic-field modulation of I_c. (c) Temperature dependence of I_c observed for a [110] junction.

most of our junctions. The exceptions were the junctions that exhibited low $J_c(\ll 10^4\ \mathrm{A/cm^2})$ and current-deficit characteristics at low temperatures as seen in Fig. 2(d), which exhibited an appreciable increase in R_n at low temperatures. In the case of an SNS junction in the clean limit, the normal resistance can be given by the Sharvin resistance $R_s = 4\pi^2\hbar^3/e^2m^2{v_F}^2DS$, where m denotes the electron effective mass, v_F is the Fermi velocity, D is the transmission probability of the interface, and S is the junction area. On the other hand, in the case of the dirty limit, the junction resistance is simply expressed as $\rho d_N/S$, where ρ is the resistivity and d_N is the thickness of the interface layer. If we assume that the interface layer has electronic properties similar to those of ion-damaged or oxygen-deficit YBCO in the metallic regime close to the metal-insulator transition, the carrier density n and the resistivity ρ in the interface layer are not far from $1\times10^{21}\ \mathrm{cm^{-3}}$ and $1\ \mathrm{m\Omega\ cm}$, respectively.[30,31] These values, together with the reasonable estimates of $v_F \sim 1\times10^7$ cm/s and $m\sim5m_e$ (m_e is the free electron mass), result in the characteristic length in the clean limit $\xi_0 (=\hbar v_F/2\pi k_B T_c)\sim1.5$ nm (for $T_c=80$ K), the mean free path $l\sim1.8$ nm, and the characteristic length in the dirty limit $\xi (=\sqrt{\xi_0 l})\sim1.7$ nm. Simple calculation using these parameters yields the Sharvin resistance for the clean limit with $D=0.5$ as $1.7\times10^{-10}\ \Omega\ \mathrm{cm^2}$ and the normal resistance of a dirty SNS junction with $d=5\xi$ as $8.5\times10^{-10}\ \Omega\ \mathrm{cm^2}$. These resistance values are considerably smaller than those observed experimentally for our IEJs, which can be seen in Fig. 4(a). This fact suggests that the Josephson current paths cover only a small fraction of the junction area. It should be noted that the junction resistance in Fig. 4(a) is thought to contain the contribution from a shunt resistor within the junction as we discussed above; thus, the actual resistance of the Josephson current path in our IEJs would be higher than those seen in the figure.

B. Characteristics of [110] junctions

Figure 7 shows the *I-V* characteristics at 4.2 K with and without an applied magnetic field [Fig. 7(a)], the Fraunhofer pattern [Fig. 7(b)], and the temperature dependence of I_c observed for a junction with the ramp edge aligned parallel to the [110] axis of the YBCO base electrode ([110] junction). This junction was fabricated under the same process conditions as those used to fabricate the standard junction, whose characteristics are shown in Figs. 2(b) and 3. Comparison with the standard junction shows that the [110] junction exhibited a 40% higher I_c at 4.2 K. This difference in the I_c values, however, is within the unavoidable run-to-run variation in our present process technology. Similarly, we could not observe any significant difference in the Fraunhofer patterns between these two types of junctions, though the [110] junction exhibited some indications of large junction behavior due to its higher I_c and a less-ideal periodic pattern in a high magnetic field. The most significant finding revealed by the comparison is that the temperature dependence of I_c in the [110] junction is exactly the same as that in the standard junction, as seen in Fig. 7(c). This definitely contradicts the theoretical prediction for clean Josephson junctions between two $d_{x^2-y^2}$-wave superconductors with perfectly flat interfaces (specular junctions).[13,14,32]

According to the formulation given by Tanaka and Kashiwaya,[14] the Josephson current in a $d_{x^2-y^2}$-wave superconductor/insulator/$d_{x^2-y^2}$-wave superconductor $(d/I/d)$ junction with [100] orientation can be described as

$$I_s(\varphi) = \frac{\pi\Delta(T)}{4eR_n}\int_{-\pi/2}^{\pi/2}\frac{\sin\varphi\cos(2\theta)}{\sqrt{1-D\sin^2(\varphi/2)}} \times\tanh\left[\frac{\Delta(T)\cos(2\theta)\sqrt{1-D\sin^2(\varphi/2)}}{2k_BT}\right]\cos\theta d\theta, \tag{1}$$

where φ is the phase difference across the junction, $\Delta(T)$ is

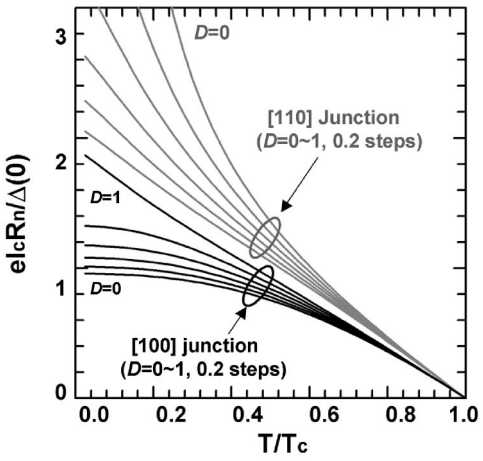

FIG. 8. I_cR_n vs T calculated by the Tanaka–Kashiwaya theory with the transmission coefficient D as a parameter. The dark lines correspond to [100] junctions and the pale lines to [110] junctions.

the order parameter in the superconductor electrodes, R_n is the normal resistance of the junction, T is the temperature, D is the transmission probability of the barrier, and θ is the angle of the quasiparticle injection relative to the junction interface normal. R_n is given by

$$R_n^{-1} = \frac{e^2}{\pi\hbar}\frac{k_F W}{\pi} D, \tag{2}$$

where k_F is the Fermi wave number and W is the junction width.

Equation (1) is similar to that for Josephson junctions made of *s*-wave superconductors, except that the angular dependence of the order parameter is taken into account. On the other hand, the Josephson current in the [110] junction can be expressed as

$$I_s(\varphi) = \frac{\pi\Delta(T)}{4eR_n}\int_{-\pi/2}^{\pi/2} \frac{\sin\,\varphi\,\sin(2\theta)}{\sqrt{D}\,\cos(\varphi/2)} \times \tanh\left[\frac{\sqrt{D}\Delta(T)\sin(2\theta)\cos(\varphi/2)}{2k_BT}\right]\cos\,\theta d\theta. \tag{3}$$

It is straightforward to calculate Eqs. (1) and (3) numerically under the assumption that $\Delta(T)$ obeys the Bardeen–Cooper–Schrieffer (BCS) theory. By maximizing $I_s(\varphi)$ with respect to φ, we can obtain the theoretical I_cR_n vs T characteristics for both the standard and [110] junctions.

Figure 8 shows the results of the calculations using Eqs. (1) and (3) with D ranging from 0 to 1.0. The dark lines represent the results for a standard [100] junction and the pale lines represent those for a [110] junction. We can see two peculiar features even for the standard junctions: smaller I_c values compared with those for conventional *s*-wave junctions and weaker saturation behavior at low temperatures. In particular, the junction in the ballistic limit ($D=1$) shows quasilinear temperature dependence over the entire temperature range. These features seem to be reasonable because the angular-averaged order parameter in *d*-wave junctions is always smaller than that in *s*-wave junctions. The behavior of the [110] junction is far more anomalous. We can see an increasing enhancement in the I_c value at low temperatures with decreasing D. This enhancement originates from the zero-energy bound states formed at the [110]-oriented junction interface.

It is evident that the specular junction model cannot explain our experimental results. We can conceive of several possible reasons for the discrepancy. The simplest idea would be that the actual junction interface is not perfectly flat but rather oriented randomly from place to place within a junction. This microscopic random orientation of junction interface would make the junction characteristics self-averaged over the angle of the local interface to the crystallographic axis, resulting in seemingly isotropic characteristics for every junction regardless of its nominal orientation. However, this simple idea alone is insufficient to explain the experimental data, because the inclusion of even a small fraction of [110]-oriented specular interface within a junction would result in divergent behavior in the I_c versus temperature characteristics at low temperatures. The only exception, as long as we accept the theoretical basis expressed by Eq. (1), is that the junction is composed of point contacts in the quantum limit with random orientation relative to the crystallographic axis. In this case, the direction of the quasiparticle injection into each point contact is restricted precisely along the normal to the interface, and thus the zero-energy bound state is not formed regardless of the relative orientation of the point contact. The Josephson current at low temperatures through each point contact making an angle α with the crystallographic a axis is approximately proportional to $\Delta(0)\cos(2\alpha)$, which vanishes for [110]-oriented interfaces ($\alpha=\pm\pi/4$). The total Josephson current is given by the sum of the current through individual point contacts, and thus we can expect nondivergent I_c vs T characteristics, similar to those of the [100]-oriented specular junctions shown in Fig. 8, regardless of the nominal orientation of the ramp edges.

Another possibility that should be addressed is the effect of disorder on the Josephson current in anisotropic superconductor junctions. Several authors have discussed the effect of interface roughness on $d/I/d$ Josephson junction characteristics.[13,33–35] Electron scattering at the rough interface broadens the zero-energy bound states, and as a consequence the anomalous temperature dependence of I_c in $d/I/d$ junctions with $\alpha\neq 0$ is smeared out. Golubov and Kupriyanov have indicated that I_c of a $d/I/d$ junction at $T=0$ scales as $\cos^2(2\alpha)$ in the regime of strong interface roughness.[34] Thus, we can expect that $d/I/d$ junctions with a rough interface of random orientation exhibit isotropic behavior without any low-temperature anomaly in their I_c vs T characteristics. Unfortunately, however, the theoretical study has also clarified that the complete suppression of the anomaly in [110]-oriented junctions simultaneously results in a significant reduction in the I_c value even for [100]-oriented junctions. This does not coincide with our experimental data.

In contrast, Asano has clarified that in the case of an SNS structure, the ensemble average of the Josephson current in [110]-oriented junctions vanishes when the N-layer is in the diffusive regime while [100] junctions with a similar N-layer exhibit a I_c value comparable with that of *s*-wave junctions.[36,37] The same author has also reported that the

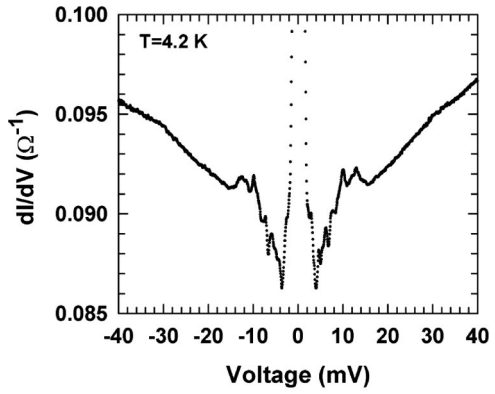

FIG. 9. Differential conductance vs voltage (dI/dV-V) characteristics at 4.2 K observed for a junction with a J_c of 3.8×10^4 A/cm^2 and an R_n of around 10 Ω.

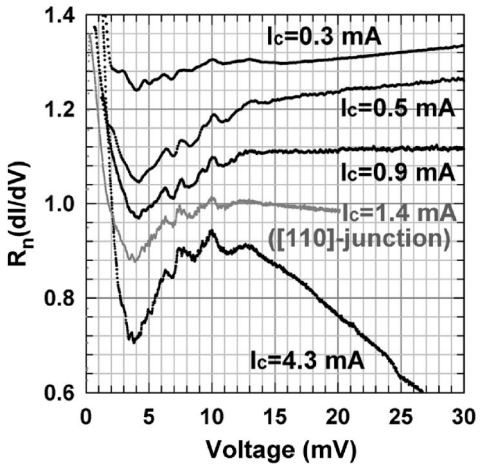

FIG. 10. Normalized differential conductance vs voltage characteristics at 4.2 K for five junctions including one with [110] orientation. The curves are shifted vertically for clarity.

disappearance of the Josephson current in [110] junctions occurs even when the N layer is in the quasiballistic regime (i.e., d_N is not much larger than the mean free path l).[38] These theoretical results lead us to another model for IEJs in which the junctions are composed of microscopic diffusive SNS junctions with random orientation. We will present a quantitative comparison of the above two junction models (the random quantum point contact model and the microscopically distributed diffusive SNS junction model) with experimental results in Sec. III D.

C. Differential conductance in IEJs

The differential conductance versus voltage (dI/dV-V) characteristics are expected to provide further information concerning the current transport in IEJs. We have measured the dI/dV-V characteristics for several junctions with different I_c values under a high magnetic field that suppresses the Josephson current. Figure 9 depicts the dI/dV profile at 4.2 K observed for a junction with an I_c of 0.3 mA ($J_c = 3.8 \times 10^4$ A/cm^2) at 4.2 K and R_n slightly greater than 10 Ω. We can see distinct fine structures in the profile below 15 mV and also some anomalies around 30 mV. We confirmed that the structures, at least those below 15 mV, were reproducible among junctions and became sharper with the increase in I_c as can be seen in Fig. 10, which shows normalized differential conductance profiles for five different junctions, including one with [110] orientation.

It has long been recognized that some microbridges made of superconductors exhibit peculiar fine structures, similar to those seen in Figs. 9 and 10, in their dI/dV profiles.[39] Klapwijk, Blonder, and Tinkham first pointed out the importance of the multiple Andreev reflection (MAR) process in such junctions, and demonstrated that the experimentally observed singularities in dI/dV profiles below the gap voltage (subharmonic gap structure, SGS) as well as the excess current at high voltages were the consequences of the MAR process.[40] A large number of successive theoretical studies have unambiguously confirmed that MAR certainly governs the current transport at finite voltages in various kinds of Josephson junctions with a highly transparent barrier. These junctions include short superconducting constrictions and SNS junctions either in the ballistic or diffusive regime.[41–45]

The MAR process manifests itself most clearly as singularities in dI/dV profiles at voltages $V_n = 2\Delta/en$, where n is an integer. Unfortunately, the fine structures below 15 mV in our junctions do not permit such simple labeling of the singularities. Moreover, in most cases, we were not able to find reproducible structures at higher voltages, though the junction shown in Fig. 10 exhibits an exceptionally weak anomaly at around 30 mV. Similar deviation from the simple MAR model has been reported for the singularities in dI/dV profiles of ramp-edge junctions with a $PrBa_2Cu_3O_7$ barrier.[46] In this case, the absence of regular periodicity in SGS has been ascribed to the existence of a reduced-T_c layer adjacent to the highly transparent tunnel barrier. The presence of such a reduced-T_c layer was also inferred for our IEJs, as discussed in Sec. III A. In addition, it is known that the amplitude and the shape of SGS in long diffusive SNS junctions depend strongly on the transparency of the SN interface, and in the case of high transparency, an appreciable SGS appears only in the dI/dV profiles.[45] This coincides with our observations, though our SGS is too weak to confirm the qualitatively different behavior for even and odd subharmonics predicted for long diffusive SNS junctions. Anyway, these facts seem to support the view that the singularities in the dI/dV profiles of our IEJs also originate from the MAR process.

Apart from the fine structures, we can see two more features in the dI/dV profiles in Fig. 10. One is the sharp rise of the differential conductance below 4 mV. We can find two plausible explanations for this phenomenon in the literature: the zero-bias anomaly due to the formation of zero-energy bound states at the interface in d-wave superconductors[47] and the $1/\sqrt{V}$ divergence of the differential conductance in disordered SNS junctions due to the Landau–Zener transitions between the Andreev bound states.[43] The former explanation, however, is contradictory to the I_c vs T characteristics of our junctions, which were discussed in the previous section. The latter explanation seems to be more likely and is consistent with the overall features of our experimental data, but the $1/\sqrt{V}$ dependence at low voltages has not been fully confirmed.

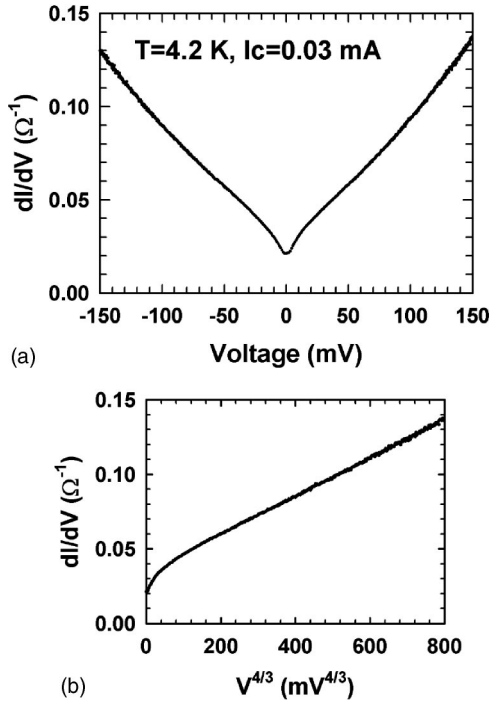

FIG. 11. (a) The dI/dV profile observed for a junction with an I_c of 0.03 mA and an R_n of 40 Ω at 4.2 K. (b) The dI/dV in the positive bias region as a function of $V^{4/3}$.

Another feature seen in Fig. 10 concerns the behavior at high voltages. The differential conductance of junctions with a I_c of less than 1 mA increases as the voltage increases, while that of junctions with a larger I_c shows the opposite behavior. The rapid decrease in dI/dV at high voltages observed in high-I_c junctions can probably be attributed to local heating, and we will not discuss this further in the present paper. On the other hand, the slight increase in dI/dV with the increase in voltage observed for junctions with a relatively small I_c requires more careful investigation, because such behavior does not always coincide with a simple SNS junction model. We think that the coexistence of "current path 2," shown in Fig. 5, within the junctions is responsible for this phenomenon.

In order to obtain further insight into the transport mechanism in path 2, we measured the dI/dV-V characteristics of an IEJ with an I_c of 0.03 mA (i.e., 3.8×10^3 A/cm^2) and R_n of 40 Ω at 4.2 K. Figure 11 depicts the results. The dI/dV profile differs considerably from those of higher-I_c junctions, and can be characterized by a slightly nonlinear increase in the conductance at high voltages, and a symmetrical dip structure with its minimum at 0 V. We found that the nonlinear behavior at high voltages was essentially independent of temperature and approximately proportional to $V^{4/3}$, as shown in Fig. 11(b). This indicates that inelastic tunneling via two localized states in the barrier plays a part in the quasiparticle transport at high voltages.[48] IEJs with R_n far exceeding 10 Ω exhibited similar characteristics. We think that this offers strong evidence that IEJs with a high normal resistance, and thus a low I_c value, have an insulator barrier with a high density of localized states in it.

It is well recognized that, in tunnel junctions with a barrier containing localized states, resonant tunneling through the localized states often dominates the quasiparticle transport at low voltages, while Cooper pairs can transfer only by direct tunneling because of the large Coulomb repulsion between two electrons on the localized states.[49] The existence of different transport channels for quasiparticles and Cooper pairs manifests itself in the different tunnel barrier thickness dependences of I_c and R_n, resulting in a peculiar relationship between I_c and R_n as R_n is proportional to I_c^{-P} and p is less than 1. If the quasiparticle current is dominated entirely by resonant tunneling, p is 0.5. This value becomes smaller when a contribution from inelastic processes via more than two localized states becomes noticeable. Generally, the relative importance of inelastic processes increases as the tunnel barrier thickness increases. Thus, we can expect a gradual decrease in p with an increase in the junction resistance. We can actually see such behavior in Fig. 3(a) for I_c values below about 0.1 mA (i.e., $J_c \leqslant 10^4$ A/cm^2). At present, we do not have direct evidence that the Josephson current in these high-resistance IEJs is governed entirely by the tunneling process. Even a small number of highly transparent point contacts embedded in an insulator barrier can offer another explanation. It is highly probable that both mechanisms coexist in junctions with an I_c of less than 0.1 mA.

The origin of the symmetrical dip around 0 V in Fig. 11 has not been clarified yet. A possible explanation may be that it is a remnant of a superconducting gap smeared out by a thin normal conducting layer or reduced T_c layer adjacent to the tunnel barrier, but a more plausible explanation is that it is an indication of the effect of the off-site Coulomb charging energy in the resonant tunneling process that has been discussed by Halbritter.[50]

It is natural to suppose that the resonant tunneling of quasiparticles via localized states in an insulator barrier, which is similar to that in high-resistance junctions, constitutes the path 2 in our low-resistance junctions. We think that the highly transparent region exhibiting the MAR process is formed dispersively in such a "dirty" insulator barrier in junctions having high I_c and low R_n values. The relative importance of the resonant tunneling process varies with the thickness and the coverage of the insulator barrier as well as with the density of the localized states, and thus depends strongly on the fabrication conditions. This results in a large variation in R_n even for junctions with similar a I_c, as we have seen in the high-I_c region in Fig. 4.

D. Junction models

In Sec. III B, we proposed two possible junction models that could explain the disappearance of the anomaly in the I_c vs T characteristics originating from the d-wave symmetry of the order parameters in [110] junctions. These are the quantum point contact (QPC) model and the microscopically distributed diffusive SNS junction model. In this section, we discuss these two junction models further.

Figure 12 shows a schematic view of our junction model. We think that the actual junction interface is a mixture of an insulator barrier with low transparency (the solid blocks in Fig. 12) and a microscopically distributed highly transparent region with random orientation relative to the crystallo-

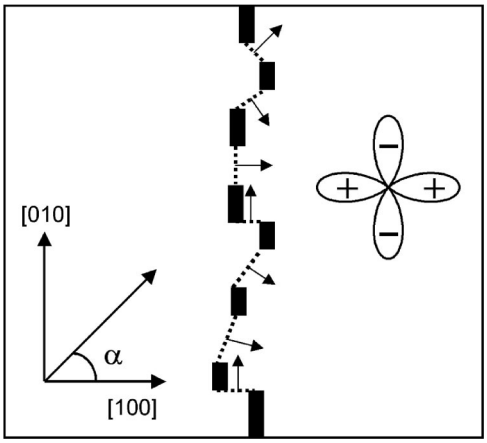

FIG. 12. Schematic view of our junction model. The solid blocks represent thick insulator barriers and the dotted areas correspond to transparent regions through which current flows. The arrows denote the direction of the current flow in each transparent region.

graphic axis (dotted-line regions in Fig. 12). The small arrows in the figure denote the direction of current flow in the transparent region. If the lateral dimensions of each transparent region are less than the Fermi wavelength (quantum point contact) and the contact length is smaller than the mean free path, current transport via a single mode is realized. The Josephson current through a quantum point contact with angle α to the crystallographic a axis can be expressed as [14]

$$I_s(\alpha,\varphi) = \frac{e\Delta(T)\cos(2\alpha)}{2\hbar}\frac{D\sin\varphi}{\sqrt{1-D\sin^2(\varphi/2)}} \times\tanh\left[\frac{\Delta(T)\cos(2\alpha)\sqrt{1-D\sin^2(\varphi/2)}}{2k_BT}\right]. \quad (4)$$

If a junction contains N point contacts with random orientation, the total current and the junction normal resistance are given by

$$I_s(\varphi) = \frac{N}{\pi}\int_{-\pi/2}^{\pi/2} I_s(\alpha,\varphi)d\alpha, \quad (5)$$

$$R_n = \frac{\pi\hbar}{e^2DN}. \quad (6)$$

The Josephson critical current can be obtained by maximizing Eq. (4) with respect to φ. Although the QPC model is sufficiently simple for use in the analysis of experimental data, it is not easy to justify its basic assumption that the dimensions of each point contact are less than the Fermi wavelength. One possibility may be that the point contacts originate from an extended localized state with a resonance width larger than Δ, for which a formula similar to Eq. (4) has been derived within the framework of conventional s-wave superconductivity.[51] However, in the case of d-wave junctions, we do not have any theoretical basis for the application of Eq. (4) to such a resonant Josephson current.

Another problem worth mentioning is that Eq. (4) is derived on the assumption that the possible spatial variation of the order parameter due to the presence of an interface can be neglected. The introduction of the spatial variation of the order parameter into the calculation of the Josephson current requires self-consistent solutions of more fundamental Green's function equations,[13,15,52] which makes it impossible to apply such an approach to the actual analysis of experimental data. Fortunately, it has been demonstrated that, although the spatial variation of the order parameter near the interface affects the magnitude of I_c, the temperature dependence of I_c remains similar to that in spatially constant order parameter cases as long as a subdominant s-wave component is not induced at the interface.[15] In the present paper, we ignore the possible inducement of an s-wave component in the order parameter at the junction interface by assuming that YBCO and YbBCO are pure d-wave superconductors and also that the disorder near the junction interface is not significant. In the QPC model, we only take into account the possible reduction of the local critical temperature T_c^* due to the disorder in the close vicinity of the junction interface.

The situation of the SNS model is more complicated. Even for conventional s-wave junctions, analytical formulas for the Josephson current in an SNS junction have been derived only for a few limited cases.[25,27] In general situations, we have to solve the Usadel equation directly under proper boundary conditions.[53] In the case of d-wave superconductors, the Green's functions contain angular-dependent order parameters; thus, the lowest order expansion of Green's functions with respect to the Fermi wave vector, which is the basic idea of the Usadel approach, is not necessarily justified. Recently, Asano investigated the case of a dirty SNS junction with a high potential barrier at the SN interfaces, and derived an analytical formula for the Josephson current component proportional to $\sin\varphi$.[37] According to the theory, the Josephson critical current of an SNS junction with an N region of length d_N can be expressed as

$$I_c(\alpha) = \frac{\pi k_BT}{e}G_N\sum_{\omega_n}[N(\alpha)]^2\frac{\ell_n}{\sinh\ell_n}, \quad (7)$$

$$N(\alpha) = \int_{-\pi/2}^{\pi/2}\frac{\Delta^-K^+}{\Xi}\cos^3\theta d\theta, \quad (8)$$

$$\Delta^{\pm} = \Delta(T)\cos[2(\alpha\mp\theta)], \quad (9)$$

$$K^{\pm} = \sqrt{\omega_n+(\Delta^{\pm})^2}-|\omega_n|, \quad (10)$$

$$\Xi = Z^2(\Delta^+\Delta^- + K^+K^-) + \cos^2\theta\Delta^+\Delta^-, \quad (11)$$

$$\ell_n = \sqrt{2n+1}\frac{d_N}{\xi_N(T)}, \quad (12)$$

where G_N is the conductance in the N region, Z denotes the strength of the barrier potential at the SN interface, $\xi_N(T) = \sqrt{\hbar D_0/2\pi k_BT}$ is the coherence length in the N region, and D_0 is the diffusion constant. Equation (7) results in a Josephson critical current approximately proportional to $|\cos(2\alpha)|$

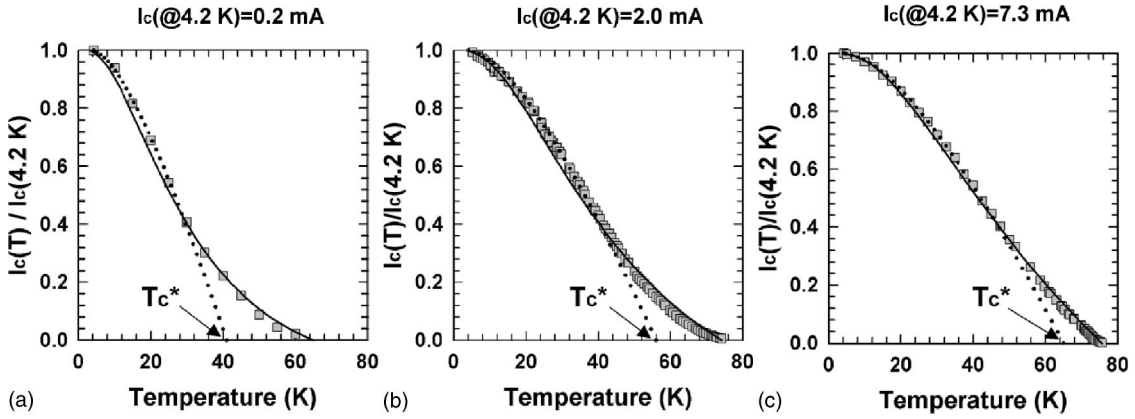

FIG. 13. Three examples of the theoretical fit to the I_c vs T characteristics. The squares represent the experimental data, and the solid and the dotted curves correspond to calculations based on the SNS and QPC junction models, respectively.

or $\cos^2(2\alpha)$ depending on the Z value, which disappears for $\alpha = \pm \pi/4$. The junction normal resistance can be described by

$$R_n = \frac{9}{4}\frac{Z^4}{G_N}. \tag{13}$$

If we assume that a junction contains N SNS contacts with random orientation and further that all the contacts are identical in terms of their area and length, then we can calculate the total Josephson critical current of the junction by simply averaging Eq. (7) over α.

One serious drawback of Eq. (7) is that it can be applied only to an SNS junction with large Z. Generally, in short SNS junctions with highly transparent SN interfaces, the current-phase relation becomes nonsinusoidal at low temperatures and the higher order harmonics of φ play a certain role in determining the Josephson critical current value. This effect is not included in Eq. (7). Experimentally, most of our IEJs exhibit high nominal J_c values ranging from 10^4 to 10^6 A/cm^2, implying that the potential barrier at the SN interfaces is not high. In the case of s-wave junctions, an analytical formula for dirty SNS junctions analogous to Eq. (7) is known to be valid only in a restricted temperature range near T_c where the Usadel function in the N layer is sufficiently small compared with $\pi k_B T$.[54,55] In spite of this difficulty, however, we adopt Eq. (7) in the following analysis to explore whether the SNS model can offer a qualitatively consistent explanation for the observed junction characteristics without expecting a precise fit to the experimental data, especially at low temperatures.

We analyzed the I_c versus temperature characteristics using the two junction models. Figure 13 shows three examples of the comparison between the experiments and the theoretical calculations. The dotted lines in the figure represent the fit of the experimental data (shown by gray squares) based on the QPC model, and the solid lines correspond to the SNS model. First, we look at the QPC model. On the assumption that the superconducting gap obeys the BCS theory, the parameters required for the fitting are the transmission coefficient D of the contact and the critical temperature T_c^* at the junction interface. Since the long tails of I_c at high temperatures due to the proximity effect are out of the scope of the QPC model, we focus only on the behavior at low temperatures. An interesting point we found through the fitting is that almost all the junctions we have analyzed so far give D values of around 0.8 independent of their absolute I_c values. Therefore, as long as we assume that the QPC model holds, we can say that all the junctions contain essentially identical point contacts. In contrast, as summarized in Fig. 14, T_c^* decreases from 65 to 40 K as I_c (at 4.2 K) decreases from 7.3 to 0.2 mA. Since this variation of T_c^* alone cannot account for the large reduction in I_c, amounting to nearly two orders of magnitude as can be seen in Fig. 14, we can also conclude that the number of point contacts within a junction varies significantly among the junctions. In contrast, the I_cR_n values, which we can calculate easily from Eqs. (5) and (6), should be independent of the number of contacts. The dark dotted line in Fig. 4(a) represents the relationship between R_n and I_c expected from the QPC model, in which the T_c^* vs I_c relation shown in Fig. 14 is taken into account. We can see that the QPC model results in a much larger I_cR_n value than observed experimentally. One possible explanation for the discrepancy may be the existence of a shunt resistor in actual junctions.

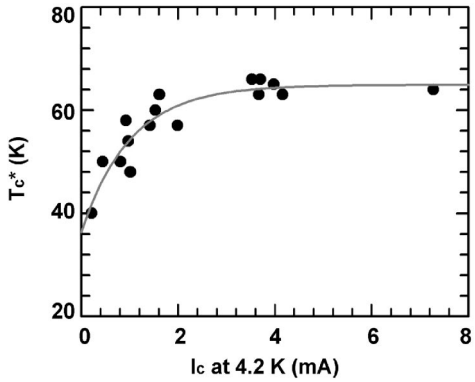

FIG. 14. Critical temperature T_c^* at the junction interface as a function of I_c at 4.2 K estimated by fitting of the experimental $I_c - T$ characteristics using the QPC model. The solid line in the figure is a guide for the eye.

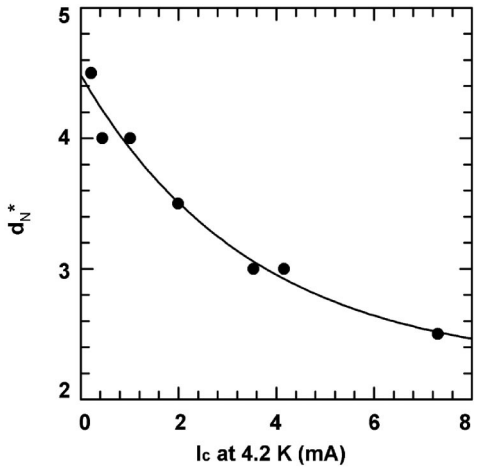

FIG. 15. Normalized contact length d_N^* vs I_c at 4.2 K estimated by fitting of the experimental I_c-T characteristics using the SNS model. The solid line in the figure is a guide for the eye.

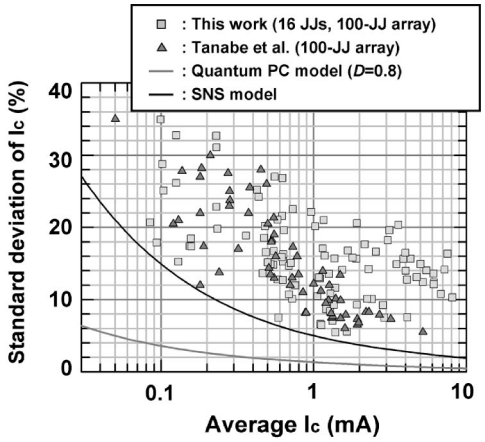

FIG. 16. Statistical fluctuation (standard deviation) of I_c observed for either 16 individual junctions in a chip or 100-junction arrays as a function of the average I_c. The dark and pale lines in the figure represent theoretical predictions by the SNS model and the QPC model, respectively.

It is worth mentioning here that in the case of *s*-wave superconductors, the Kulik–Omelyanchuk theory[56] for diffusive point contact in the short length limit ($d_N \ll \xi$) results in I_c vs T characteristics similar to those in the case of clean point contacts with a transmission coefficient of about 0.8. If the analogy is possible for *d*-wave superconductors, the universal D value observed for our IEJs may suggest that the point contacts in IEJs should be regarded as diffusive ones rather than QPCs in an atomic scale. Unfortunately, we do not have a firm theoretical basis for extending this idea further at present.

Fitting using the SNS model requires three parameters: the normalized junction length d_N^* defined as $d_N^*=d_N/\xi_n(T_c)$, the strength of the barrier potential Z, and the critical temperature T_c. We assumed T_c to be the temperature where the experimental Josephson current in individual junctions vanishes. In most cases, this critical temperature was slightly lower than those observed for the bulk electrodes. We fixed Z at 1.0 *a priori* throughout the present analysis based on our observation that the shape of the I_c vs T curve is rather insensitive to Z. Thus, in practice, we varied only d_N^* to find the point where a satisfactory agreement between the calculation and the experiment was obtained. The results are shown in Fig. 13 by solid lines. When we take into account the limited validity of Eq. (7), the SNS model seems to work quite well. In fact, we can see that the tail region near T_c is reproduced reasonably well by the model. The d_N^* values estimated by the fitting varied from 2.5 to 4.5 depending on the I_c values at 4.2 K, as shown in Fig. 15. This variation in d_N^* is again too small, as was the case of T_c^* in the QPC model, to account for the variation in the I_c values. Thus, even in the framework of the SNS model, we can conclude that the number of the contacts within a junction area plays a significant role in determining the absolute I_c value.

The reasonable agreement of the experimental I_c vs T characteristics with Eq. (7), together with the weak SGS in the dI/dV profiles discussed in the previous section, suggests that the SNS model would give a better description of IEJs compared with the QPC model. However, the present SNS model results in I_cR_n values almost one order of magnitude smaller than the experimental values, as indicated by the pale dotted line in Fig. 4(a). At present, we are not sure whether an extension of Eq. (7) to more general cases for arbitrary Z and d_N can resolve this discrepancy or not. An advanced self-consistent theory for SNS junctions in which the *d*-wave symmetry of the order parameter, the proximity effect at the SN interface, and the effect of the elastic scattering in the N region are fully taken into account is required. However, this is far beyond the scope of the present paper.

Finally, we discuss the statistical fluctuation of I_c within the framework of the present junction models. The fluctuation of I_c is of critical importance for the digital circuit applications of high-temperature superconductor Josephson junctions. Figure 16 shows the standard deviation σ of I_c as a function of the average I_c observed for junctions on a large number of wafers. The σ values were derived either for 16 single junctions on a chip or for a 100-junction series array. Similar data reported by Tanabe *et al.*[57] are also plotted for comparison. We can see that the data from two independent laboratories exhibit a common tendency, indicating that Fig. 16 depicts an important feature of IEJs. Empirically, the σ value varied from wafer to wafer even if the process conditions were kept as constant as possible. We can conceive of various origins for the σ variation, and most of them are technology dependent. One example is differences in the density of precipitates on the surface of the isolation layer originating from the slight deviation of the atomic composition from the stoichiometry of the YBCO base electrode located underneath the isolation layer.[22] We have confirmed that the σ value correlates strongly with the precipitate density. However, even if the precipitate density was reduced to a sufficiently low level, σ differences ranging from several % to a few tens of % of I_c remained depending on the average I_c value. We think some inherent mechanism exists in IEJs that restricts further reduction of the σ value. Thus we will focus only on the behavior of the minimum σ as a function of the average I_c seen in Fig. 16.

As we discussed above, the I_c value is primarily determined by the number of contacts within a junction. The variation of T_c^* in the framework of the QPC model or that of d_N^* in the SNS model is of secondary importance. A natural consequence of this is that the σ value would be governed by the fluctuation in the number of contacts within a junction. In the following, we will confirm this idea quantitatively.

Within the QPC model, I_c at low temperatures of a single point contact with angle α can be expressed approximately as

$$I_c(\alpha) \approx \frac{e\Delta(T)\cos(2\alpha)}{2\hbar} f(D), \tag{14}$$

where $f(D)=1.1$ for $D=0.8$. Then, the ensemble average of the critical current $\langle I_c \rangle$ and the standard deviation σ relative to $\langle I_c \rangle$ for junctions containing N point contacts with random orientation are given by

$$\langle I_c \rangle = \frac{N}{\pi} \frac{e\Delta(T)}{\hbar} f(D) = 0.35N \frac{e\Delta(T)}{\hbar}, \tag{15}$$

$$\sigma = \frac{1}{2}\sqrt{\frac{\pi}{2} - \frac{4}{\pi}} \sqrt{\frac{e\Delta(T)f(D)}{\hbar}} \langle I_c \rangle^{-1/2} = 0.29 \sqrt{\frac{e\Delta(T)}{\hbar}} \langle I_c \rangle^{-1/2}. \tag{16}$$

It is straightforward to calculate σ at 4.2 K as a function of $\langle I_c \rangle$ using Eq. (16) by taking into account the empirical relation between T_c^* and I_c in Fig. 14. The result is shown in Fig. 16 by the pale line. The calculated σ is considerably smaller than the experimental value in the whole I_c range. Therefore, as long as we assume that the QPC model holds, we still have a good opportunity to further reduce the σ value.

On the other hand, in the case of the SNS model with $Z=1$, I_c of a single contact at low temperatures can be expressed approximately as

$$I_c(\alpha) \approx I_c(\alpha = 0)\cos^2(2\alpha). \tag{17}$$

Hence, $\langle I_c \rangle$ and σ become

$$\langle I_c \rangle = N \frac{I_c(\alpha = 0)}{2}, \tag{18}$$

$$\sigma = \frac{\sqrt{I_c(\alpha = 0)}}{2} \langle I_c \rangle^{-1/2}. \tag{19}$$

In contrast to the QPC model, we cannot calculate the absolute σ value directly without the knowledge of the area of the contact. However, if we fix σ at a given $\langle I_c \rangle$ to a certain value, we can know the behavior of σ in the whole $\langle I_c \rangle$ range by using the d_N^* versus I_c relation in Fig. 15 together with Eq. (9). The dark line in Fig. 16 represents σ as a function of $\langle I_c \rangle$ when we assume that σ at $\langle I_c \rangle = 1$ mA is 5%. The calculated line reproduces the experimentally observed behavior fairly well. Since Eq. (19) is equivalent to $\sigma = 1/\sqrt{2N}$, $\sigma = 5\%$ corresponds to $N=200$. Thus, according to Eq. (18), a single contact with $\alpha = 0$ in a junction with an $\langle I_c \rangle$ of 1 mA carries a Josephson current of 10 μA. This value, together with a reasonable estimate of the physical parameters in the N region such as $\rho = 1$ mΩ cm and $D_0 = 1$ cm^2/s, enables us to estimate the area of the single contact using Eq. (7). The estimated value is 9×10^{-12} cm^2. Although this contact area seems to be feasible, we have to bear in mind that the present SNS model probably underestimates the Josephson critical current value, and thus overestimates the junction area, as we discussed above. In spite of this uncertainty, however, the reasonable agreement between the calculation and the experiment seen in Fig. 16 is impressive and confirms that the fluctuation in the number of microscopic SNS contacts within a junction certainly restricts the attainable minimum spread of the I_c value.

IV. SUMMARY AND CONCLUSION

We have presented a comprehensive study of the transport mechanisms in interface-engineered Josephson junctions fabricated from high-temperature superconductors based on more than 1000 junctions with excellent Josephson characteristics. No appreciable difference in junction characteristics was observed between junctions with [100]- and [110]-aligned ramp edges, indicating that some self-averaging mechanism that smears out the effect of the *d*-wave pairing symmetry on the Josephson current exists within the junction. We have shown that a microscopically distributed diffusive SNS junction model based on the Asano theory is a possible candidate to explain the overall features of the experimentally observed junction characteristics. This model reproduces the I_c vs T characteristics reasonably well for a wide range of junctions, and is also consistent with our experimental observations of the relatively high excess current and the weak subharmonic gap structure due to multiple Andreev reflections for junctions with J_c exceeding 10^4 A/cm^2. This model, however, results in an I_cR_n value that is nearly one order of magnitude smaller than that observed experimentally. This is probably due to the limited validity of the Asano theory, in which only the Josephson current component proportional to sin ϕ is taken into account. Further advancement of the theory for SNS junctions, in which both the angular-dependent order parameter and the proximity effect are treated self-consistently, is required to fully understand the experimental results quantitatively. An important finding of the present study is that the statistical fluctuation of I_c is governed mainly by the fluctuation of the number of microscopic SNS contacts within a junction area. In spite of the large variation in experimental I_c, which exceeded three orders of magnitude, the variation in the length of the SNS contacts seems to be of secondary importance.

We have also shown that microscopic SNS contacts are embedded dispersively in an insulator barrier containing a large number of localized states. Resonant tunneling of quasiparticles through the localized states constitutes a shunt resistor within a junction. The contribution of the resonant tunneling path differs appreciably even for junctions with a similar I_c value. This results in a large variation of R_n even for junctions with similar I_c. All these phenomena, which we

have observed through transport measurements, are probably related closely to the recrystallization mechanism of the junction interface during the counter-electrode deposition process, and may have some relation with the recently reported inhomogeneous superconducting state in disordered superconductors.[58,59] Unfortunately, we do not have sufficient data concerning the atomic structure of the junction interface and its relation to the transport properties. A closer investigation by TEM combined with transport measurement may provide further information.

ACKNOWLEDGMENTS

We are grateful to M. Yu. Kupriyanov for critical reading of the manuscript and helpful discussion concerning the validity of the Asano model. We are also indebted to K. Tanabe for kindly providing the data plotted in Fig. 16. This work was supported by the New Energy and Industrial Technology Development Organization (NEDO) as Collaborative Research and Development of Fundamental Technologies for Superconductor Applications.

[1] B. H. Moeckly and K. Char, Appl. Phys. Lett. **71**, 2526 (1997).
[2] J. Yoshida, IEICE Trans. Electron. **E83-C**, 49 (2000), and references therein.
[3] T. Satoh, M. Hidaka, and S. Tahara, IEEE Trans. Appl. Supercond. **9**, 3141 (1999).
[4] T. Suzuki, Y. Ishimaru, M. Horibe, O. Horibe, H. Wakana, S. Adachi, Y. Oshikubo, Y. Tarutani, U. Kawabe, and K. Tanabe, Physica C **392–396**, 1378 (2003).
[5] J. G. Wen, N. Koshizuka, S. Tanaka, T. Satoh, M. Hidaka, and S. Tahara, Appl. Phys. Lett. **75**, 2470 (1999).
[6] Y. Huang, K. L. Merkle, B. H. Moeckly, and K. Char, Physica C **314**, 36 (1999).
[7] Y. Soutome, T. Fukazawa, T. Tsukamoto, Y. Tarutani, and K. Takagi, in *Advances in Superconductivity XII*, edited by T. Yamashita and K. Tanabe (Springer, Tokyo, 2000), p. 990.
[8] Y. Wu, Y. Ishimaru, H. Wakana, S. Adachi, Y. Tarutani, and K. Tanabe, J. Appl. Phys. **92**, 4571 (2002).
[9] Y. Ishimaru, Y. Wu, T. Suzuki, M. Horibe, O. Horibe, H. Wakana, S. Adachi, Y. Tarutani, and K. Tanabe, Physica C **392–396**, 1373 (2003).
[10] J. K. Heinsohn, R. Dittmann, J. Rodriguez Contreras, J. Scherbel, A. Klushin, M. Siegel, C. J. Lia, A. A. Golubov, and M. Yu. Kupriyanov, J. Appl. Phys. **89**, 3852 (2001).
[11] J. Yoshida, H. Katsuno, S. Inoue, and T. Nagano, Physica C **367**, 260 (2002).
[12] S. Yip, Phys. Rev. B **52**, 3087 (1995).
[13] Yu. S. Barash, H. Burkhardt, and D. Rainer, Phys. Rev. Lett. **77**, 4070 (1996).
[14] Y. Tanaka and S. Kashiwaya, Phys. Rev. B **56**, 892 (1997).
[15] Y. Tanaka and S. Kashiwaya, Phys. Rev. B **58**, R2948 (1998).
[16] G. Koren, E. Polturak, N. Levy, and G. Deutscher, Phys. Rev. B **61**, 3734 (2000).
[17] H. Arie, K. Yasuda, H. Kobayashi, I. Iguchi, Y. Tanaka, and S. Kashiwaya, Phys. Rev. B **62**, 11 864 (2000).
[18] E. Ilichev, M. Grajcar, R. Hlubina, R. P. J. Ijsselsteijn, H. E. Hoenig, H. G. Meyer, A. Golubov, M. H. S. Amin, A. M. Zagoskin, A. N. Omelyanchouk, and M. Yu. Kupriyanov, Phys. Rev. Lett. **86**, 5369 (2001).
[19] P. V. Komissinski, B. Hogberg, A. Y. Tzalenchuk, and Z. Ivanov, Appl. Phys. Lett. **80**, 1022 (2002).
[20] F. Lombardi, F. Tafuri, F. Ricci, F. MilettoGranozio, A. Barone, G. Tests, E. Sarnelli, J. R. Kirtley, and C. C. Tsuei, Phys. Rev. Lett. **89**, 207001 (2002).
[21] M. Sigrist and T. M. Rice, J. Phys. Soc. Jpn. **61**, 4283 (1992).
[22] H. Katsuno, S. Inoue, T. Nagano, and J. Yoshida, Appl. Phys. Lett. **79**, 4189 (2001).
[23] H. Katsuno, S. Inoue, T. Nagano, and J. Yoshida, IEEE Trans. Appl. Supercond. **13**, 809 (2003).
[24] A. Barone and G. Paterno, *Physics and Applications of the Josephson Effect* (Wiley, New York, 1982), Chap. 5.
[25] For a review article, see K. K. Likharev, Rev. Mod. Phys. **51**, 101 (1979).
[26] J. Yoshida, H. Katsuno, K. Nakayama, S. Inoue, and T. Nagano, IEEE Trans. Appl. Supercond. **13**, 599 (2003).
[27] For a review article, see A. A. Golubov, M. Yu. Kupriyanov, and E. Il'ichev, Rev. Mod. Phys. **76**, 411 (2004).
[28] A. A. Golubov and M. Yu. Kupriyanov, Sov. Phys. JETP **69**, 805 (1989).
[29] A. A. Golubov, V. M. Krasnov, and M. Yu. Kupriyanov, J. Low Temp. Phys. **106**, 249 (1997).
[30] J. M. Valles, Jr., A. E. White, K. T. Short, R. C. Dynes, J. P. Garno, A. F. J. Levi, M. Anzlowar, and K. Baldwin, Phys. Rev. B **39**, 11 599 (1989).
[31] K. Semba and A. Matsuda, Phys. Rev. Lett. **86**, 496 (2001).
[32] R. A. Riedel and P. F. Bagwell, Phys. Rev. B **57**, 6084 (1998).
[33] A. A. Golubov and M. Yu. Kupriyanov, JETP Lett. **67**, 501 (1998).
[34] A. A. Golubov and M. Yu. Kupriyanov, JETP Lett. **69**, 262 (1999).
[35] A. Poenicke, Yu. S. Barash, C. Bruder, and V. Istyukov, Phys. Rev. B **59**, 7102 (1999).
[36] Y. Asano, Phys. Rev. B **63**, 052512 (2001).
[37] Y. Asano, Phys. Rev. B **64**, 014511 (2001).
[38] Y. Asano, Physica C **367**, 157 (2002).
[39] P. E. Lindolf, Rep. Prog. Phys. **44**, 949 (1981).
[40] T. M. Klapwijk, G. E. Blonder, and M. Tinkham, Physica B & C **109B**, 1657 (1982).
[41] K. Flensberg, J. B. Hansen, and M. Octavio, Phys. Rev. B **38**, 8707 (1988).
[42] G. B. Arnold, J. Low Temp. Phys. **68**, 1 (1987).
[43] A. Bardas and D. V. Averin, Phys. Rev. B **56**, R8518 (1997).
[44] A. V. Zaitsev and D. V. Averin, Phys. Rev. Lett. **80**, 3602 (1998).
[45] E. V. Bezuglyi, E. N. Bratus, V. S. Shumeiko, G. Wendin, and H. Takayanagi, Phys. Rev. B **62**, 14 439 (2000).
[46] A. Engelhardt, R. Dittmann, and A. I. Braginski, Phys. Rev. B **59**, 3815 (1999).
[47] Y. Tanaka and S. Kashiwaya, Phys. Rev. Lett. **74**, 3451 (1995).
[48] L. I. Glazman and K. A. Matveev, Sov. Phys. JETP **67**, 1276 (1988).
[49] R. Gross, L. Alff, A. Beck, O. M. Froehlich, D. Koelle, and A.

Marx, IEEE Trans. Appl. Supercond. **7**, 2929 (1997).
[50] J. Halbritter, Phys. Rev. B **46**, 14 861 (1992).
[51] L. I. Glazman and K. A. Matveev, JETP Lett. **49**, 650 (1989).
[52] M. Fogelstrom, S. Yip, and J. Kurkijarvi, Physica C **294**, 289 (1998).
[53] K. D. Usadel, Phys. Rev. Lett. **25**, 507 (1970).
[54] M. Yu. Kupriyanov and V. F. Lukichev, Sov. Phys. JETP **67**, 1163 (1988).
[55] M. Yu. Kupriyanov (private communications).
[56] I. O. Kulik and A. N. Omelyanchuk, JETP Lett. **21**, 96 (1975).
[57] K. Tanabe, H. Wakana, S. Adachi, H. Sugiyama, Y. Ishimaru, M. Horibe, T. Machi, K. Suzuki, and Y. Tarutani (unpublished).
[58] A. Ghosal, M. Randeria, and N. Trivedi, Phys. Rev. B **65**, 014501 (2001).
[59] Z. Wang, J. R. Engelbrecht, S. Wang, H. Ding, and S. H. Pan, Phys. Rev. B **65**, 064509 (2002).